Deuteron-induced reactions on ^{9}Be, ^{10}B, and ^{11}B at low energies

Jingsheng Yan, F. E. Cecil, J. A. McNeil, and M. A. Hofstee
Department of Physics, Colorado School of Mines, Golden, Colorado 80401

P. D. Kunz
Department of Physics, University of Colorado, Boulder, Colorado 80309-0446

(Received 1 October 1996)

We have measured angular distributions and total cross sections for the reactions (d,p) and (d,α) to all excited states with positive Q-values on the nuclei ^{9}Be, ^{10}B, and ^{11}B between center of mass (c.m.) energies of 57 and 139 keV, 67 and 141 keV, and 76 and 144 keV, respectively, and the reaction (d,t) on the nucleus ^{9}Be to the ^{8}Be ground state between c.m. energies of 57 and 139 keV. Astrophsyical S factors for these reactions are derived from the total cross-section measurements. Some of the measured angular distributions are far from isotropic even at the lowest energies. This anisotropy is reproduced reasonably well by distorted-wave Born approximation calculations in which the distorting potentials are modified with an additional short-range term. [S0556-2813(97)04004-1]

PACS number(s): 24.10.−i, 25.45.Hi, 25.60.Dz

I. INTRODUCTION

Deuteron-induced reactions on light nuclei have been the object of extensive investigation throughout the history of nuclear physics. The deuteron-induced reactions on deuterium, tritium, and ^{3}He, for example, have been well measured at low energies [1,2]. The interest in these particular reactions is based upon their role as the fundamental energy producing reactions in the current generation of fusion plasma experiments and their being possible examples of the Oppenheimer-Phillips effect [3] or the influence of electron screening on nuclear reaction rates at very low energies [4]. Similarly, a detailed study of the deuteron-induced reactions on ^{6}Li has been reported [5], motivated in part by the role played by these reactions in some of the advanced fusion plasma fuel cycles. There has, however, been no systematic investigation of the total and differential cross sections for the deuteron-induced reactions on ^{7}Li, ^{9}Be, ^{10}B, or ^{11}B at low energies.

We believe such an investigation is well justified on the basis of the role played by these reactions in several areas of applied physics, such as tokamak fusion plasma devices, as well as basic nuclear reaction theory. For example, the first walls of TFTR and JET are layered in boron and beryllium, respectively. First wall contamination of the fusion plasmas constitutes an inevitable source of power loss and the nuclear reactions between these contaminants and the deuterium fuel may provide the basis for a diagnostic of this contamination through the noninvasive spectrometry of the associated reaction γ rays [6]. These reactions may likewise play a crucial role in the study of primordial nucleosynthesis. The ^{3}He and triton induced reactions on ^{7}Li have been discussed as sources of ^{9}Be within the context of the standard big bang [7]. Such production opens up a network of deuteron-induced reactions on the isotopes of Be and B leading, in principle, to the synthesis of the CNO elements. The cross sections for the deuteron-induced reactions on the isotopes of beryllium and boron must then be known for energies in the 100 to 200 keV range if the nucleosynthesis within this network is to be quantified.

In addition to these areas of applied physics, these reactions may be used to test nuclear reaction theories at low energies. While R-matrix theory, for example, has proved quite successful in the analysis of d-d reactions at low energies [8], this approach is only now being applied to deuteron-induced reactions on heavier nuclei [9]. Consequently, a comprehensive measured set of total and differential cross sections for such reactions should prove extremely useful in the evaluation of these theoretical efforts. Alternatively, it would be of interest to investigate whether the distorted-wave Born approximation (DWBA), which has proved so successful in the study of nuclear reactions at higher energies throughout the periodic table, could find application on light nuclei at very low energies. Traditionally, direct reactions at very low energies have had, in general, to compete with compound nuclear reactions. However, for the very light nuclei under consideration in the present work, the level densities in the compound systems are extremely low and the possibility of understanding the differential and total cross sections in terms of a direct reaction mechanism, such as the DWBA, must be given serious consideration.

In the next section, we present our experimental techniques and the results of our measurements of the total and differential cross sections for all the positive Q-value deuteron-induced reactions on the nuclei ^{9}Be, ^{10}B, and ^{11}B for center of mass energies between about 50 and 150 keV. Since all of these energies are well below the respective Coulomb barriers, we use the measured total cross sections to extract the corresponding astrophysical S factors. In the last section, we compare the measured differential cross sections to cross sections calculated in the DWBA. In the course of this investigation, we have also measured the ^{7}Li$+d$ reactions at low energies. Because of the competition between the two-body final state $\alpha+{}^{5}$He and the direct three-body final state $2\alpha+n$, the analysis of this reaction is considerably more complex than the deuteron reactions on ^{9}Be, ^{10}B, and

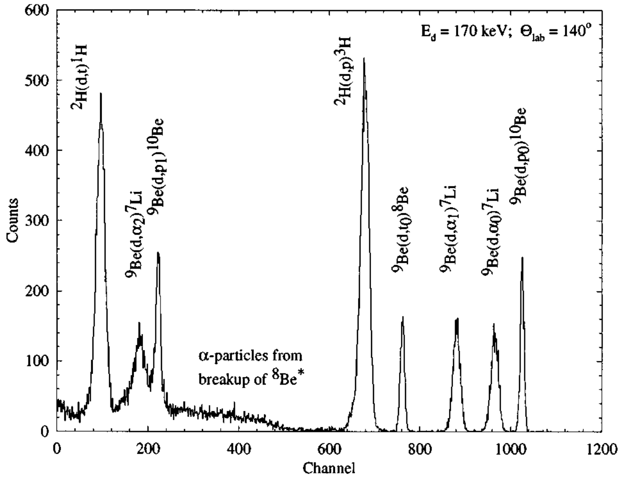

FIG. 1. An energy spectrum of the charged particles produced by deuteron bombardment of a thick beryllium target. The ground state Q values for the (d,p), (d,α), and (d,t) reactions on ^{9}Be are 4.587, 4.592, and 7.151 MeV, respectively.

^{11}B. Consequently our measurement of the $^{7}\mathrm{Li}+d$ reaction will be described in a separate report.

II. EXPERIMENTAL PROCEDURE

The experiments consisted of bombarding thick targets of the appropriate material with magnetically analyzed deuteron beams and measuring the energy spectra of the charged particles from the induced nuclear reactions. All the experiments were carried out on the low-energy, high-current charged-particle accelerator [10], General Ionex model 1545, housed in the Nuclear Physics Laboratory at the Colorado School of Mines. The accelerator beam energy was calibrated by the known resonance of $^{11}\mathrm{B}(p,\alpha)^{9}\mathrm{Be}$ [11,12]. The energy spread of the beam is less than 1 keV [10] since the quoted stability of the accelerator system is about 100 eV, and since the beam line was operated at a pressure of 10^{-7} torr.

A scattering chamber of 27-cm diameter was used in all the experiments. The targets were mounted in target holders and were 360° turnable. The accelerated beams were focused into spots of about 6-mm diameters at the center of targets after passing through an aluminum collimator. A 90 V potential was used for secondary electron suppression [13].

The targets for $^{9}\mathrm{Be}+d$ reaction were a plate of pure (purity $>$99%) beryllium metal with a polished surface, and the targets used in $^{10}\mathrm{B}+d$ and $^{11}\mathrm{B}+d$ reactions were made by pressing 90%-enriched ^{10}B powder and natural boron powder (purity $>$99%) into target holders of 3$\sim$4-cm diameters, respectively.

The reaction charged particles were measured with silicon surface-barrier detectors which were covered with 1-μm Ni foils to stop the intense flux of elastically scattered particles from targets. In measurements of angular distributions, active windows of detectors and detector telescopes were limited by slit apertures, typically $\sim 3.5\times 14$ mm^{2}. Detectors could be rotated from 0° to 160° and the beam was centered on the rotation axis to within about 3 mm. The accuracy in angular positions was estimated to be $\pm 2°$.

Because of target heating, it was not considered feasible to measure the reactions using targets sufficiently thin that the reactions would be occurring at well defined energies. Consequently the measurements were made with targets which were thick compared to the ranges of the bombarding deuterons (the range of 180 keV deuterons in Be or B is about 1 μm while the targets were typically $\simeq$1-mm thick). The advantage of using these thick targets is, as implied above, that the targets can sustain a much greater heat load than thin targets. The disadvantages are, first, that the reaction products can only be measured in reflection geometry (at scattering angles greater than about 60°) and, secondly, that the measured yields represent an integral of yields between the incident beam energy and zero energy. In the case of the first problem, angular distributions were measured between scattering angles of about 60° to 160° and fit to low order polynomial distributions which allowed extrapolation to more forward angles with reasonable confidence in order to extract total cross sections and hence astrophysical S factors. Because of the second problem, the measured yield (detected counts per incident deuteron) at a given bombarding energy E_0 and scattering angle Θ must be expressed in terms of the energy dependent total cross section $\sigma(E)$ as an integral:

$$Y(E_0,\Theta)=\frac{\Omega_d}{4\pi}n_t\int_0^{E_0}\frac{\sigma(E)}{\chi(E)}W(E,\Theta)dE, \tag{1}$$

where $W(E,\Theta)$ is the angular distribution normalized so that its integral over all solid angles is 4π, Ω_d is solid angle of the detector relative to the target, n_t is the number density of the target nuclei, and $\chi(E)$ is the stopping power of the target material.

Assuming the angular distributions are slowly varying functions of energy relative to the cross sections, the angular distributions can be factored from the integral in Eq. (1):

$$Y(E_0,\Theta)\simeq W(E_0,\Theta)\frac{\Omega_d}{4\pi}n_t\int_0^{E_0}\frac{\sigma(E)}{\chi(E)}dE. \tag{2}$$

TABLE I. Summary of the thick-target angular distributions for the $^{9}\mathrm{Be}+d$ reaction measured at the two c.m. energies.

Reaction	w_1(90 keV)	w_2(90 keV)	w_1(123 keV)	w_2(123 keV)
$^{9}\mathrm{Be}(d,p_0)^{10}\mathrm{Be}$(g.s.)	-0.97 ± 0.11	not used	-0.788 ± 0.037	not used
$^{9}\mathrm{Be}(d,p_1)^{10}\mathrm{Be}^*$(3.3680 MeV)	-0.34 ± 0.10	not used	-0.272 ± 0.044	not used
$^{9}\mathrm{Be}(d,t_0)^{8}\mathrm{Be}$(g.s.)	-0.34 ± 0.14	-0.39 ± 0.21	-0.617 ± 0.090	-0.349 ± 0.093
$^{9}\mathrm{Be}(d,\alpha_0)^{7}\mathrm{Li}$(g.s.)	-0.374 ± 0.070	not used	-0.175 ± 0.027	not used
$^{9}\mathrm{Be}(d,\alpha_1)^{7}\mathrm{Li}^*$(0.47761 MeV)	$+0.472\pm0.039$	not used	$+0.268\pm0.032$	not used

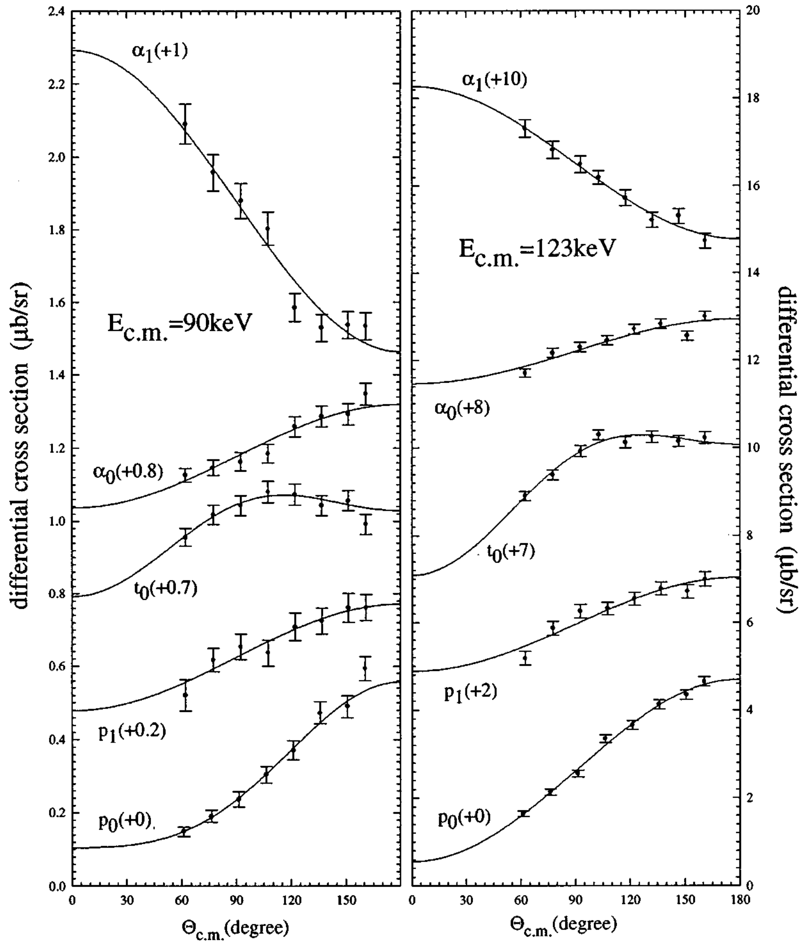

FIG. 2. The thick-target angular distributions for the measured particle groups from ^{9}Be+d reaction at two energies. The error bars are statistical only and the solid curves represent least squares fits to the data points. Note that the data points and the curves (but not the error bars) have been added by the numbers in the parentheses to be plotted. Thus for the reactions (d,α_1) in this figure, the fitted angular distribution has a maximum at 0° of 1.30 μb/sr and a minimum at 180° of 0.46 μb/sr.

Since all of the quantities on the right-hand side of Eq. (2) are independent of angle except for the normalized angular distributions $W(E,\Theta)$, a measurement of the thick-target yields $Y(E_0,\Theta)$ will allow a determination of the corresponding normalized angular distributions $W(E_0,\Theta)$.

In the case of the ^{9}Be and ^{11}B measurements, the angular distributions were each measured at two energies and these sets of measurements were used to parametrize the angular distributions over the c.m. energy ranges from the minimum (70 and 90 keV, respectively) up to the maximum energies (132 and 140 keV, respectively). Our assumption that the angular distributions $W(E_0,\Theta)$ are slowly varying functions of energy is supported *a posteriori*. In the case of the ^{10}B we assumed that the angular distributions are constant between c.m. energies of 72 and 138 keV.

Once the angular distributions are determined, Eq. (2) can be used to determine the total cross sections $\sigma(E)$. This was done using two different methods.

Method I. The total cross section can be described by the S factor $S(E)$ as

$$\sigma(E)=\frac{S(E)}{E}e^{-\sqrt{E_G/E}}, \qquad (3)$$

where E_G is the Gamow energy

$$E_G=\frac{2\mu\pi^2e^4Z_1^2Z_2^2}{\hbar}=0.989Z_1^2Z_2^2\mu \quad (\mathrm{MeV}), \qquad (4)$$

where μ is the target projectile reduced mass in amu. Using Eq. (3), Eq. (2) can then be expressed as

$$Y(E_0,\Theta)=\frac{\Omega_d}{4\pi}n_tW(E_0,\Theta)\int_0^{E_0}\frac{S(E)}{E\chi(E)}e^{-\sqrt{E_G/E}}dE. \qquad (5)$$

The thick-target yield is measured at a fixed angle for a series of energies E_i. The parameters of an assumed functional form of the S factor may then be determined by integrating numerically the right-hand side of Eq. (5) and fitting these values to the measured thick-target yields. In the present work, since there are no significant (sharp) resonances [14,15] for the reactions under investigation between c.m. energies of 50 and 150 keV, a simple quadratic polynomial dependence for the S factor is assumed.

Method II. If the difference between E_i and E_{i-1} is sufficiently small, Eq. (2) may be used to determine approximately the cross section at an energy E_{eff} between E_i and E_{i-1}:

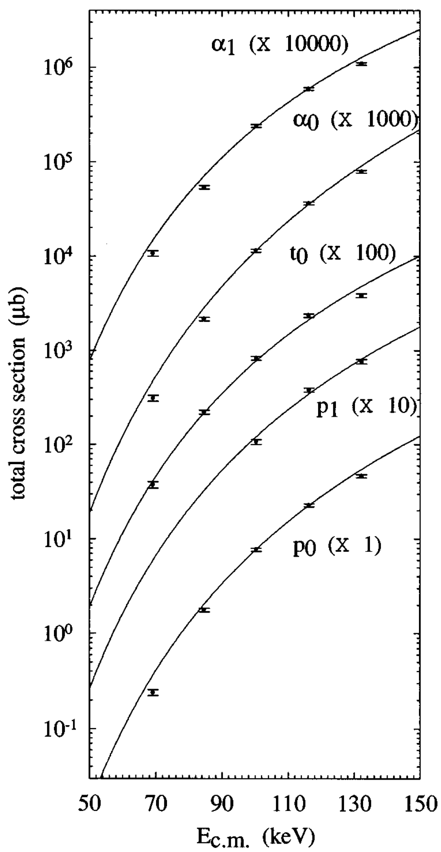

FIG. 3. The total cross sections for the measured particle groups from ^{9}Be+d reaction. The solid curves are obtained from fitting the measured thick-target yields in Method I and the data points result from Method II (the curves are not direct fits to the data points). Note that the curves, data points, and the error bars have been multiplied by the numbers in the parentheses to be plotted.

$$\sigma(E_{\text{eff}})=\frac{4\pi\chi(E_{\text{eff}})}{\Omega_d n_t W(E_{\text{eff}},\Theta)}\,\frac{Y_i-Y_{i-1}}{E_i-E_{i-1}}, \tag{6}$$

where E_{eff} is the appropriately weighted effective c.m. energy calculated between E_i and E_{i-1}, and given by

$$\int_{E_{i-1}}^{E_i}\frac{1}{E\chi(E)}e^{-\sqrt{E_G/E}}dE=2\int_{E_{\text{eff}}}^{E_i}\frac{1}{E\chi(E)}e^{-\sqrt{E_G/E}}dE,$$

$$(E_i>E_{i-1}), \tag{7}$$

and where $W(E_{\text{eff}},\Theta)$ is the thick-target angular distribution obtained at E_{eff} and averaged at Θ over Ω_d.

Once the total cross sections $\sigma(E)$ are determined, the differential cross sections are given by

$$\frac{d\sigma}{d\Omega}=\frac{1}{4\pi}W(E,\Theta)\sigma(E). \tag{8}$$

III. EXPERIMENTAL RESULTS

A. The ^{9}Be+d reaction

Figure 1 illustrates an energy spectrum of charged particles measured during the deuteron bombardment of the beryllium target. The deuterium accumulation in the thick targets will produce the proton and triton peaks from the ^{2}H(d,p) ^{3}H reaction.

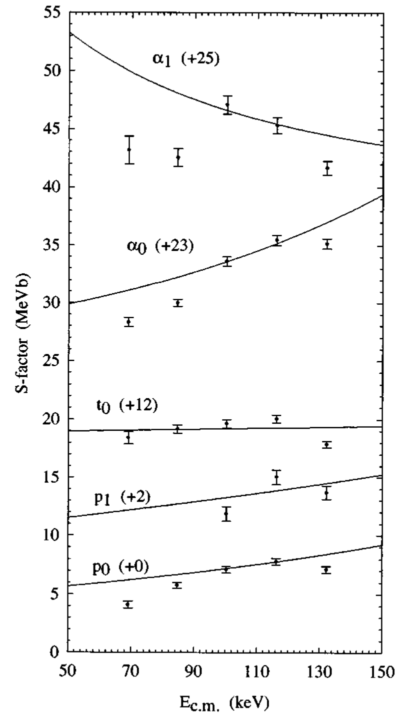

FIG. 4. The S factors for the measured particle groups from ^{9}Be+d reaction. As discussed in the text the solid curves are from Method I and the data points are calculated from the values of total cross sections in Method II. The curves are not the direct fits of the data points. Note that the curves and the data points (but not the error bars) have been added by the numbers in the parentheses to be plotted.

The thick-target angular distributions were measured at two deuteron bombarding energies of 110 and 150 keV and are fitted to

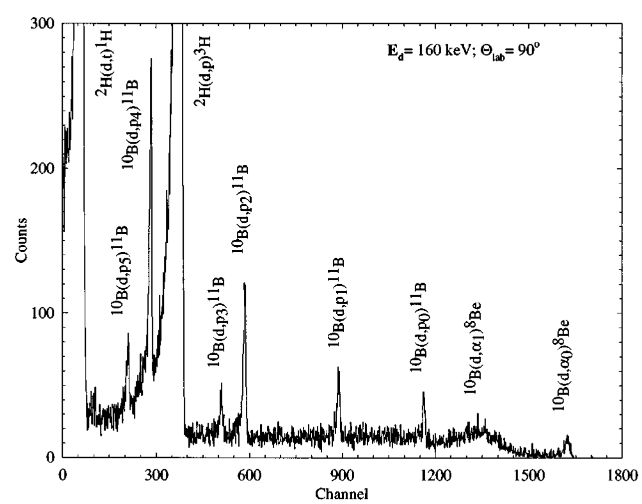

FIG. 5. An energy spectrum of the charged particles produced by deuteron bombardment of a thick 90%-enriched ^{10}B target. The ground-state Q values for the (d,p) and (d,α) reactions on ^{10}B are 9.231 and 17.821 MeV, respectively.

TABLE II. Summary of the thick-target angular distributions for the ^{10}B$+d$ reaction measured at 133 keV c.m. energy.

Reaction	w_1(133 keV)	w_2(133 keV)
^{10}B$(d,p_0)^{11}$B(g.s.)	-0.45 ± 0.14	-0.22 ± 0.14
^{10}B$(d,p_1)^{11}$B*(2.1247 MeV)	not used	-0.223 ± 0.080
^{10}B$(d,p_2)^{11}$B*(4.4451 MeV)	$+0.808\pm0.035$	-0.250 ± 0.034
^{10}B$(d,p_3)^{11}$B*(5.021 MeV)	not used	-0.51 ± 0.14
^{10}B$(d,p_4)^{11}$B*(6.743 MeV)	not used	not used
^{10}B$(d,p_5)^{11}$B*(7.286 MeV)	not used	not used
^{10}B$(d,\alpha_0)^{8}$Be(g.s.)	-0.0572 ± 0.059	-0.390 ± 0.067
^{10}B$(d,\alpha_1)^{8}$Be*(3.04 MeV)	-0.580 ± 0.043	-0.184 ± 0.046

$$W(E_i,\Theta)=1+w_1(E_i)P_1(\cos\Theta)+w_2(E_i)P_2(\cos\Theta). \qquad (9)$$

The coefficients $w_1(E_i)$ and $w_2(E_i)$ (for $i=1,2$) are given in Table I. The measured angular distributions are shown in Fig. 2. The coefficients w_1 and w_2 are determined at each of the two energies using only the relative angular distributions. Using the methods described above, the total cross sections were determined and then, using Eq. (8), the absolute differential cross sections are determined which are plotted in Fig. 2. Our measurements are consistent with previous measurements of the relative angular distributions for the reactions ^{9}Be$(d,p_0)^{10}$Be(g.s.) [16,17], ^{9}Be$(d,t_0)^{8}$Be(g.s.) [16], ^{9}Be$(d,\alpha_0)^{7}$Li(g.s.) [17], and ^{9}Be$(d,\alpha_1)^{7}$Li* (0.47761 MeV) [17].

In order to use the two methods discussed previously to extract the cross sections, the thick-target angular distributions at the two energies have to be extrapolated to the narrow energy region of the present work. For the purposes of this extrapolation we assumed w_1 and w_2 to be linear func-

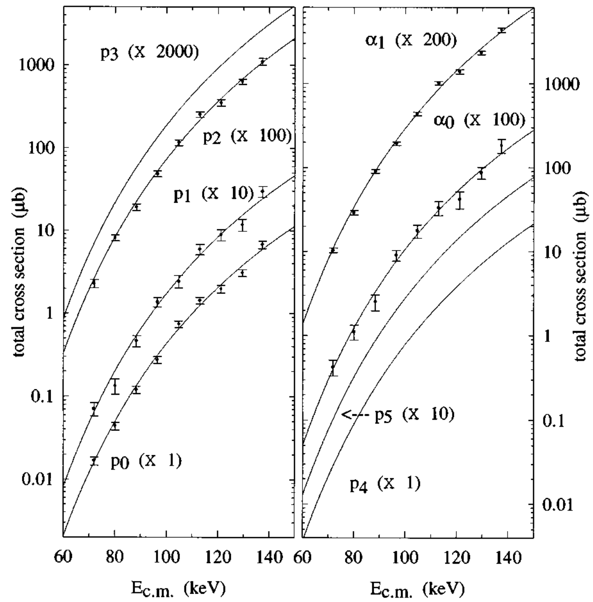

FIG. 7. The total cross sections for the measured particle groups from ^{10}B$+d$ reaction. As discussed in the text the solid curves are obtained from fitting the measured thick-target yields in Method I and the data points result from Method II (the curves are not direct fits to the data points). Note that the curves, data points, and the error bars have been multiplied by the numbers in the parentheses to be plotted. For the p_3, p_4, p_5 groups, the excitation functions were measured at a single deuteron energy and constant S factors were assumed, hence, no data point can be obtained by Method II.

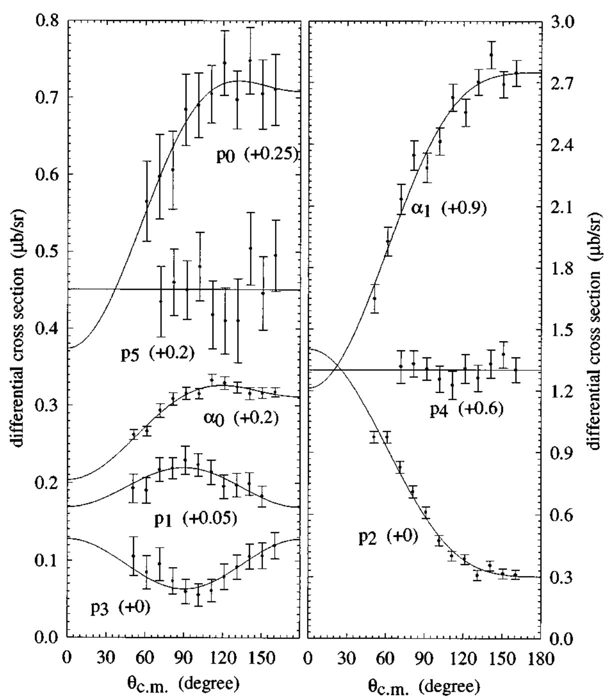

FIG. 6. The thick-target angular distributions for the measured particle groups from ^{10}B$+d$ reaction. The error bars are statistical only and the solid curves represent least squares fits to the data points. Note that the data points and the curves (but not the error bars) have been added by the numbers in the parentheses to be plotted.

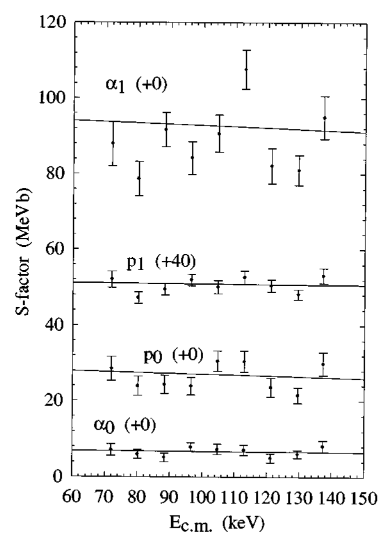

FIG. 8. The S factors for the measured particle groups for the ^{10}B$+d$ reactions to the ground and the first excited states. As discussed in the text the solid curves are from Method I and the data points are calculated from the values of total cross sections in Method II. The curves are not the direct fits of the data points. Note that the curves and the data points (but not the error bars) have been added by the numbers in the parentheses to be plotted. The S factors of the p_2, p_3, p_4, p_5 groups can be obtained from the total cross sections in Fig. 7.

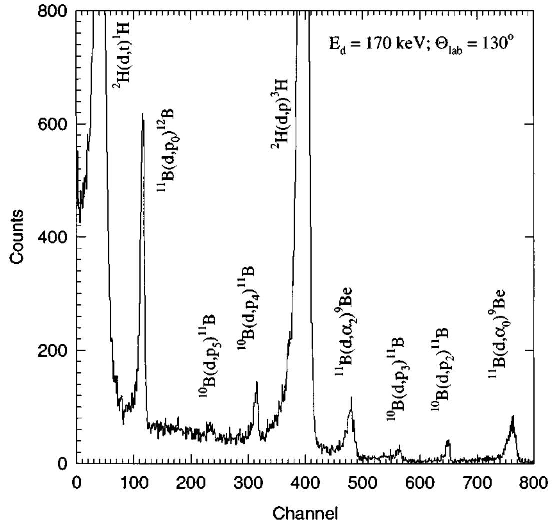

FIG. 9. An energy spectrum of the charged particles produced by deuteron bombardment of a thick natural boron target. The ground-state Q values for the (d,p) and (d,α) reactions on ^{11}B are 1.144 and 8.030 MeV, respectively.

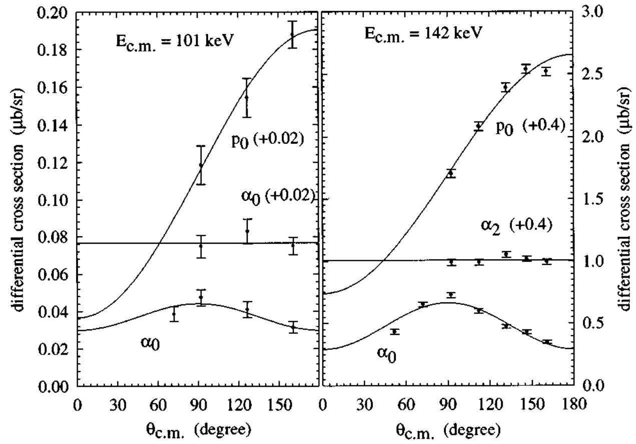

FIG. 10. The thick-target angular distributions for the measured particle groups from ^{11}B$+d$ reaction at two energies. The error bars are statistical only and the solid curves represent least squares fits to the data points. Note that the data points and the curves (but not the error bars) have been added by the numbers in the parentheses to be plotted.

tions of energy and used the values from Table I to determine the coefficients of these linear functions.

The excitation functions were measured at an angle of 140° in the laboratory system with deuteron c.m. energies between 57 and 139 keV. Figures 3 and 4 plot the measured total cross sections and the S factors calculated from the cross sections using Eq. (3), respectively, where the solid lines are calculated by Method I while the data points were extracted using Method II. We remind the reader that each data point in Figs. 2 and 3 (and in the corresponding figures for the ^{10}B and ^{11}B reactions) is derived from two adjacent thick-target yield points [recall Eq. (6)]. Consequently, while the thick-target yields were measured at seven deuteron c.m. energies ranging from 57 to 139 keV, the cross sections were deduced at six values of the intermediate effective c.m. energies [Eq. (7)] ranging from 70 to 132 keV. It is these six values of the cross section and corresponding S factors that are plotted in Figs. 3 and 4. For this reaction as well as for the ^{10}B$+d$ and ^{11}B$+d$ reactions discussed below, the solid lines are not fits of the data points but represent the alternative extraction process.

B. The ^{10}B$+d$ reaction

Figure 5 presents an energy spectrum of charged particles measured during the deuteron bombardment of the 90%-enriched ^{10}B target. Again, the proton and triton peaks from the ^{2}H$(d,p)^3$H reaction occur due to deuterium accumulation in the thick target.

The thick-target angular distributions were measured at a deuteron bombarding energy of 160 keV and were fit to Eq. (9) ($i=1$ only). The coefficients $w_1(E_i)$ and $w_2(E_i)$ are given in Table II. Figure 6 shows these measured angular distributions. As with the beryllium results, the angular distributions are given in terms of the differential cross sections. From the energy levels [14] of ^{12}C (the compound nucleus for the ^{10}B$+d$ reaction), one notes that all the resonances in this reaction in the energy region of the present work are very broad with the widths full width at half maximum of 2000, 510, and 920 keV, compared with the present c.m. energy region of 60 to 150 keV. Therefore we assume the functions w_1 and w_2 in Eq. (9) are constant over the energy range of the present work and we used the angular distributions at $E_{\mathrm{c.m.}}=133$ keV to evaluate these constants.

The excitation functions of the reactions ^{10}B(d,p_0) ^{11}B(g.s.), ^{10}B(d,p_1) ^{11}B*(2.1247 MeV), ^{10}B(d,p_2)^{11}B* (4.4451 MeV), ^{10}B(d,α_0) ^{8}Be(g.s.), and ^{10}B(d,α_1) ^{8}Be* (3.04 MeV) were measured at an angle of 90° in the lab. system with deuteron bombarding energies between 80 and 170 keV. Figure 7 plots the measured total cross sections with the solid lines obtained using Method I and the data points obtained using Method II. For the reactions ^{10}B(d,p_3) ^{11}B*(5.021 MeV), ^{10}B(d,p_4) ^{11}B*(6.743 MeV), and ^{10}B(d,p_5) ^{11}B*(7.286 MeV), the excitation functions were measured at a single deuteron energy and a constant S factor for each reaction was assumed, hence, no data points could be obtained by Method II. The upper limit of the energy range of our measurements of the total cross sections of

TABLE III. Summary of the thick-target angular distributions for the ^{11}B$+d$ reaction measured at the two c.m. energies.

Reaction	w_1(101 keV)	w_2(101 keV)	w_1(142 keV)	w_2(142 keV)
^{11}B$(d,p_0)^{12}$B(g.s.)	-0.82 ± 0.17	not used	-0.737 ± 0.039	not used
^{11}B$(d,\alpha_0)^8$Be(g.s.)	not used	-0.241 ± 0.089	not used	-0.460 ± 0.027
^{11}B$(d,\alpha_2)^8$Be*(2.429 MeV)	not used	not used	not used	not used

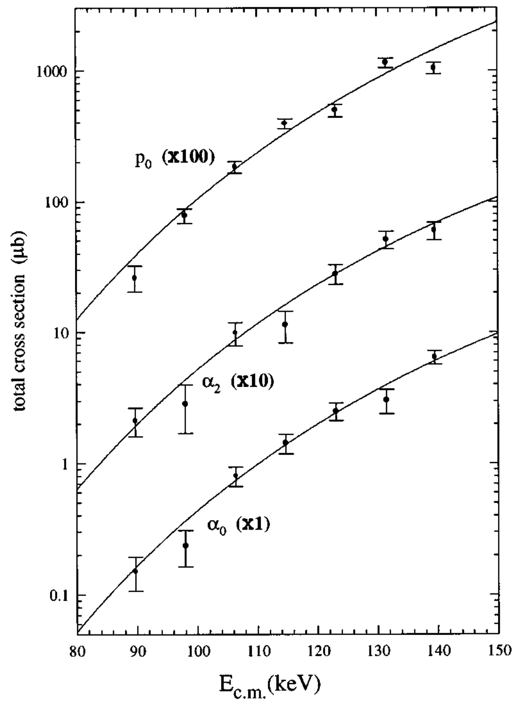

FIG. 11. The total cross sections for the measured particle groups from ^{11}B$+d$ reaction. As discussed in the text the solid curves are obtained from fitting the measured thick-target yields in Method I and the data points result from Method II (the curves are not direct fits to the data points). Note that the curves, data points and the error bars have been multiplied by the numbers in the parentheses to be plotted.

the reactions ^{10}B(d,p_0)^{11}B(g.s.), ^{10}B(d,p_1)^{11}B*(2.1247 MeV), ^{10}B(d,p_2)^{11}B*(4.4451 MeV), and ^{10}B(d,p_3)^{11}B*(5.021 MeV) overlap the lower limit of the energy range of Ref. [18], and our measurements agree with those of Ref.

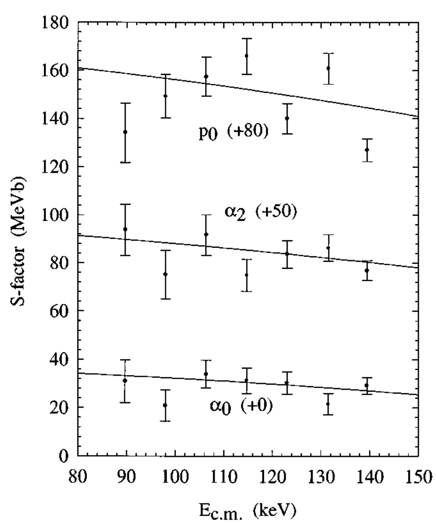

FIG. 12. The S factors for the measured particle groups from ^{11}B$+d$ reaction. As discussed in the text the solid curves are from Method I and the data points are calculated from the values of total cross sections in Method II. The curves are not the direct fits of the data points. Note that the curves and the data points (but not the error bars) have been added by the numbers in the parentheses to be plotted.

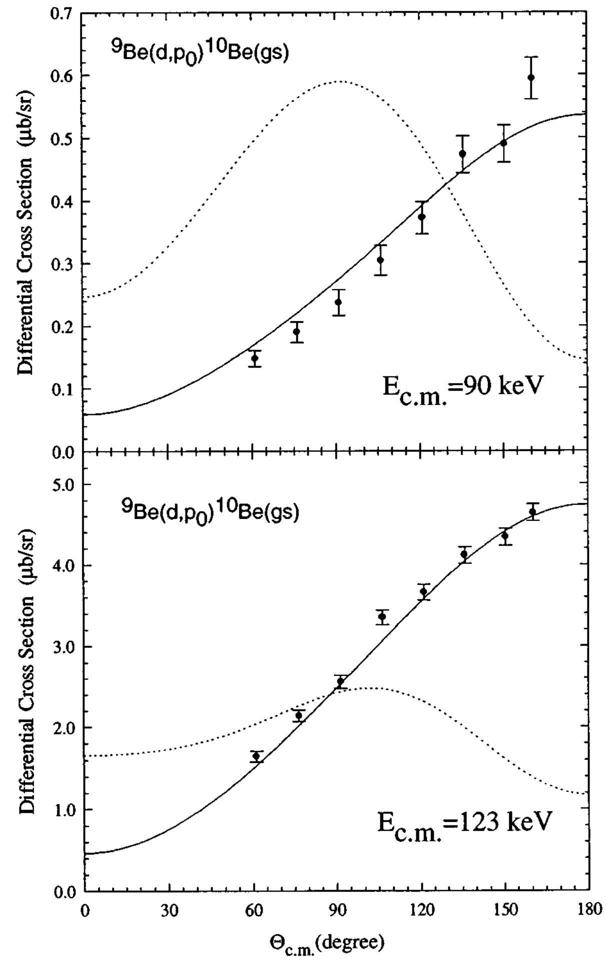

FIG. 13. Results of DWUCK4 calculations for the reaction ^{9}Be(d,p_0)^{10}Be(g.s.) at c.m. energies of 90 and 123 keV. The data points are measured in this work. The solid curves are calculated including a short-range modification to the distorting potentials to simulate symmetrization effects while the dotted curves represent the same calculations without the modified potentials. The spectroscopic factor was extracted from the overall scale. The parameters are listed in Table IV.

[18] in this overlap region. The S factors have been obtained from the measured total cross sections. Figure 8 gives the S factors for the reactions to the ground state and the first excited state. The S factors for the other excited states in ^{11}B can be obtained from the measured cross sections in Fig. 7 using Eq. (3).

C. The ^{11}B$+d$ reaction

An energy spectrum of charged particles measured during the deuteron bombardment the natural boron target is shown in Fig. 9. The ^{2}H(d,p)^{3}H reaction is again evident as well as reactions from the ^{10}B in the target.

The thick-target angular distributions were measured at deuteron bombarding energies of 120 and 168 keV and were fit to Eq. (9) $(i=1,2)$. As with the ^{9}Be measurements, the coefficients w_1 and w_2 are assumed to be linear functions of energy based on the values given in Table III. Figure 10 shows the measured c.m. differential cross sections.

TABLE IV. DWUCK distorting potential parameters (see Ref. [20] for definitions of the parameters). The volume Wood-Saxon potential (option 1) (with the imaginary part set to zero) was used throughout. The second line for each case lists the values of the s-wave modification potential parameters. The (in)/(out) refer to the entrance and exit channels. Spectroscopic factors extracted from the overall scale of the calculated cross sections are given in the second column.

Reaction	S_{lsj} (exp)	Channel	V_R (MeV)	r_0 (fm)	A_0 (fm)
^{9}Be (d,p_0)	0.92	(in)	-81	1.15	0.58
			$+130$	0.81	0.10
		(out)	-57	1.15	0.58
			$+116$	0.60	0.10
^{9}Be (d,t_0)	0.96	(in)	-92	1.15	0.58
			$+130$	0.81	0.10
		(out)	-120	1.15	0.58
			$+95$	0.60	0.10
^{10}B (d,p_0)	0.78	(in)	-96	1.15	0.58
			$+130$	0.81	0.10
		(out)	-70	1.15	0.58
			$+114$	0.60	0.10
^{11}B (d,p_0)	1.62	(in)	-81	1.15	0.58
			$+130$	0.81	0.10
		(out)	-81	1.15	0.58
			$+116$	0.60	0.10

The excitation functions were measured at 130° in the lab system with deuteron beam energies between 100 and 170 keV. Figures 11 and 12 plot the measured total cross sections and the S factors, respectively, where again the solid lines are obtained using Method I and the data points are obtained using Method II.

IV. DISTORTED-WAVE BORN APPROXIMATION ANALYSIS

In order to understand better the physical mechanisms involved in the deuteron-induced reactions studied here, we have undertaken a series of DWBA calculations. Low-energy nuclear physics lore has it that more sophisticated approaches, such as the resonating group method [19], are considered more appropriate for this energy regime. Nevertheless the simpler direct reaction mechanism approximated by the distorted wave approach may offer at least qualitative insights. We make use of the DWUCK4 code described in Ref. [20] where the DWBA cross section in fm^2 for the reaction $A(d,p)B$, where $B=A+n$ is given in zero-range approximation by

$$\frac{d\sigma^{lsj}(\Theta)}{d\Omega}=\frac{2J_B+1}{2J_A+1}\,\frac{S_{lsj}}{2j+1}\,\frac{D_0^2}{10^4}\,\sigma_{DW}^{lsj}(\Theta), \qquad (10)$$

where $\sigma_{DW}^{lsj}(\Theta)$ is the calculated cross section described in detail in Ref. [20], S_{lsj} is the spectroscopic factor which we will extract from the overall scale of the data, and D_0^2 is the effect of folding the interaction over composite projectile and/or ejectile wave functions as described in Ref. [22] which further estimates $D_0^2 \simeq 1.58\times 10^4$ MeV^2 fm C^3 for (d,p) and $D_0^2 \simeq 2.3\times 10^4$ MeV^2 fm C^3 for (d,t).

First, consider the ^{9}Be (d,p_0) ^{10}Be (g.s.) reaction at $E_{\mathrm{c.m.}}=90$ and 123 keV. The DWBA calculation is shown as the dotted lines in Fig. 13. The agreement is quite poor, which is especially problematic considering that we have allowed the potential parameters to vary in an attempt to describe the data. In particular the shape of the angular distributions are dramatically different from those measured. This perhaps suggests that the reaction mechanism may not in fact be a simple one-step direct reaction as assumed implicitly by the DWBA formalism. Another possibility is that an essential piece of the relevant physics has been omitted which, while strictly speaking lies outside the scope of DWBA, can still be simply modeled in the DWBA context. Such is the case with Pauli blocking which can usually be safely ignored at higher energies, but which is crucial at these very low energies where the identity of the projectile and target particles surely has a significant impact on the effective distorting potential.

The resonating group calculations, such as those of Fujiwara and Tang [21], correctly incorporate antisymmetrization, however, their calculations require significant extensions from their present configuration (such as the inclusion of Coulomb distortions) to be applied here. We are investigating other resonating group codes to test on our data. The distorted wave code DWBA70 [23] incorporates antisymmetrization but is limited to (p,p') applications. We are not aware of any properly antisymmetrized DWBA codes that deal with transfer reactions, and a properly antisymmetrized calculation is beyond the scope of this work. However, to test the plausibility of our hypothesis, we have simulated the effect of the symmetrization by including an additional potential term of a range appropriate to the bound s-wave target nucleons (i.e., short ranged) and with a strength of roughly that of the attractive potential (per particle). This modifies the short-range part of the distorting potential more than the other channels. The parameters of this additional term were adjusted at one energy and then used to calculate the cross

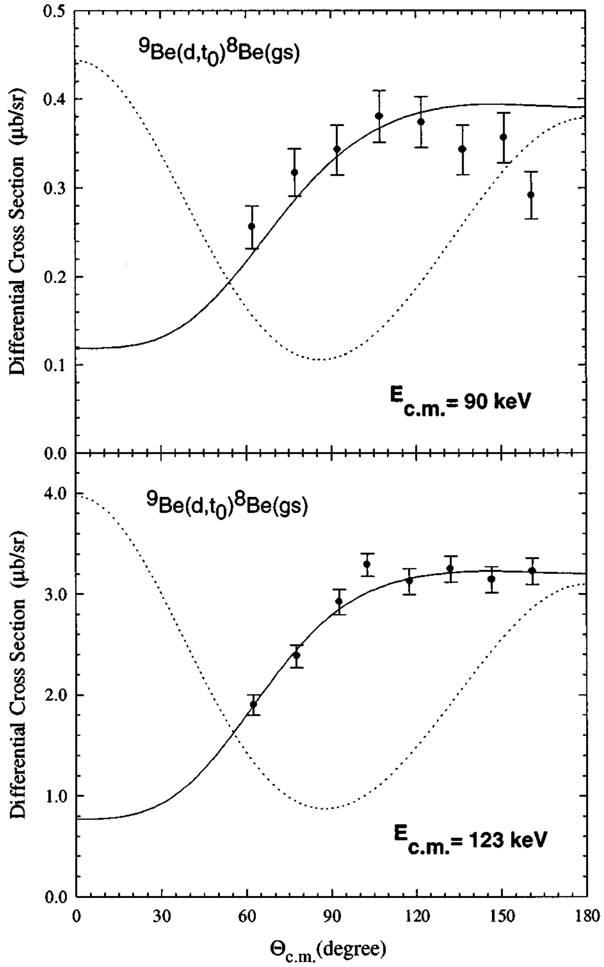

FIG. 14. Same as Fig. 13 for the reaction ^{9}Be$(d,t_0)\,^{8}$Be(g.s.).

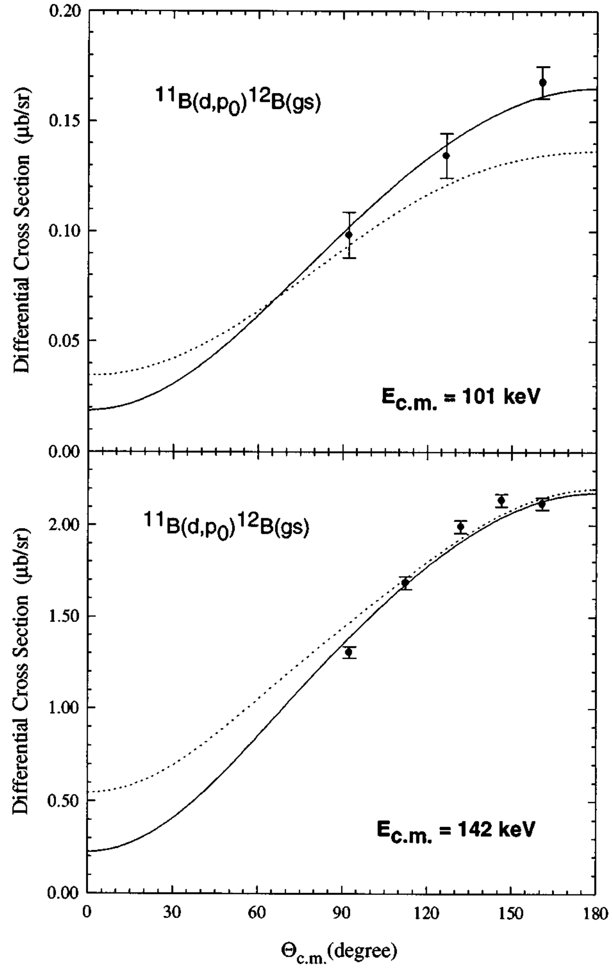

FIG. 16. Same as Fig. 13 for the reaction ^{11}B$(d,p_0)\,^{12}$B(g.s.).

section at another energy without further adjustment. The results of the modified DWBA calculations for the ^{9}Be (d,p_0) ^{10}Be(g.s.) reaction at $E_{\text{c.m.}}=90$ and 123 keV are shown as the solid curve in Fig. 13. The short-range modifi-

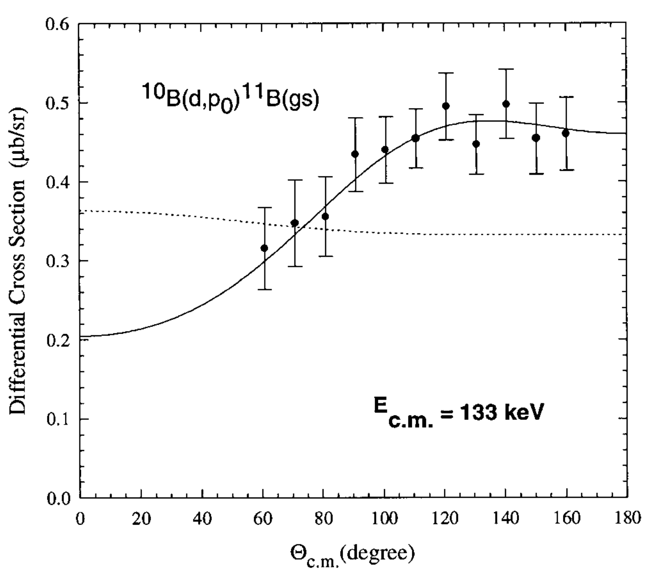

FIG. 15. Same as Fig. 13 for the reaction ^{10}B$(d,p_0)\,^{11}$B(g.s.).

cation parameters and overall scale were adjusted to the 90 keV measurements, but not changed in the 123 keV calculation. The resulting angular distributions are in good agreement with the measured cross section suggesting, but not proving, that we are on the right track. The specific DWUCK4 parameters for the distorting potentials as well as the extracted spectroscopic factors for this reaction and for the ^{9}Be (d,t_0) ^{8}Be(g.s.) and the ^{11}B (d,p_0) ^{11}B(g.s.) reactions are listed in Table IV.

A similar procedure was carried out for the ^{9}Be (d,t_0) ^{8}Be(g.s.) reaction at $E_{\text{c.m.}}=90$ and 123 keV the results of which are presented in Fig. 14. Again the dotted curve shows a standard DWBA calculation without modifying the short-range distorting potential while the solid curve indicates the striking improvement that arises from modification of the short-range part of the distorting potentials. Figure 15 considers the ^{10}B (d,p_0) ^{11}B(g.s.) reaction at $E_{\text{c.m.}}=133$ keV and again the modification of the short-range distorting potential results in substantial improvement of the theoretical descriptions of the angular distributions.

Finally, Fig. 16 considers the ^{11}B (d,p_0) ^{11}B(g.s.) reaction at $E_{\text{c.m.}}=101$ and 142 keV. Unlike the previous examples, the unmodified DWBA calculation is in reasonable agreement with the data. Not surprisingly, including a short-range modification to the distorting potential results in a modest improvement of the theoretical descriptions of the angular distributions.

We wish to emphasize that our calculations only suggest that symmetrization effects incorporated with a direct reaction mechanism approximated by the distorted-wave born approximation *may* provide a sufficient understanding of these reactions. Indeed the parameters used for the short-range modifications are not unique and do not connect directly with any fundamental theory. In fact one can alter these potential strength and range parameters of either the incoming or exiting channels such that the volume integrals are constant without affecting the results significantly. Without doing a properly antisymmetrized calculation, one cannot be more definitive.

V. DISCUSSION AND CONCLUSIONS

In summary, we have completed a survey of total cross sections and angular distributions for all the charged particle producing, exothermic deuteron-induced reactions on the nuclei ^{9}Be, ^{10}B, and ^{11}B at center of mass energies between about 70 and 140 keV. As noted in our introduction, one area of application of the measurements will be to the problem of primordial nucleosynthesis. Specifically, the reactions ^{7}Li(He,p)^{9}Be and ^{7}Li$(t,n)^9$Be have been proposed as a mechanism for the production of ^{9}Be in the big bang and the present measurements supply part of the data base for investigating the primordial production of heavier elements, including carbon starting with ^{9}Be. In order to complete this data base, it would be necessary to know the neutron producing reactions within this network. There are presently no complete measurements of the (d,n) reactions on these nuclei in this energy range. We are planning to carry out such a series of measurements in the near future in an effort to complete our knowledge of this reaction network. In addition to these astrophysical applications, we would also like to stress the nature of our measured angular distributions. Specifically we found a remarkable degree of anisotropy throughout the measurements and that this anisotropy was well reproduced by DWBA calculations in which an *ad hoc* short-range term is added to the nucleon-nucleus potential. At present the interpretation of this term is not clear and we plan to continue our investigation of this phenomenon.

ACKNOWLEDGMENT

This work supported in part by the U.S. DOE.

[1] R. E. Brown and N. Jarmie, Phys. Rev. C **41**, 1391 (1990).
[2] A. Krauss *et al.*, Nucl. Phys. **A465**, 150 (1987).
[3] J. R. Oppenheimer and M. Phillips, Phys. Rev. **48**, 500 (1935).
[4] S. Engstler *et al.*, Phys. Lett. B **279**, 20 (1992).
[5] A. J. Elwyn *et al.*, Phys. Rev. C **16**, 1744 (1977).
[6] S. S. Medley, F. E. Cecil, D. Cole, M. A. Conway, and F. J. Wilkinson, Rev. Sci. Instrum. **56**, 975 (1985).
[7] T. Kajino and R. N. Boyd, Astrophys. J. **359**, 267 (1990).
[8] G. M. Hale, R. E. Brown, and N. Jarmie, Phys. Rev. Lett. **59**, 763 (1987).
[9] G. M. Hale (private communication).
[10] F. E. Cecil, D. Ferg, R. King, B. Kriss, H. Liu, and J. Scorby, Nucl. Inst. Methods Phys. Res. B **40/41**, 934 (1989).
[11] J. M. Davidson *et al.*, Nucl. Phys. **A315**, 253 (1979).
[12] H. W. Becker, C. Rolfs, and H. P. Trautvetter, Z. Phys. A **327**, 341 (1987).
[13] Jinsheng Yan, Ph.D. thesis, Colorado School of Mines, 1995.
[14] F. Ajzenberg-Selove, Nucl. Phys. **A433**, 1 (1985).
[15] F. Ajzenberg-Selove, Nucl. Phys. **A449**, 1 (1986).
[16] R. K. Smither, Phys. Rev. **107**, 196 (1957).
[17] G. Ambrosino, J. P. Crettez, J. Lachkar, and J. Perchereau, J. Phys. (Paris) Colloq. **1**, 62 (1966).
[18] G. R. Harrison, G. d. Schmidt, and C. D. Curtis, Phys. Rev. **117**, 532 (1960).
[19] J. A. Wheeler, Phys. Rev. **52**, 1083 (1937); **52**, 1107 (1937); see also, G. Blüge and K. Langanke, *Advances in Nuclear Physics*, edited by J. W. Negele and E. Vogt (Plenum, New York, 1993), Vol. 21.
[20] P. D. Kunz and E. Rost, in *Computational Nuclear Physics*, edited by K. Langanke, J. A. Maruhn, and S. E. Koonin (Springer-Verlag, New York, 1993), Vol. 2, Chap. 5.
[21] Y. Fujiwara and Y. C. Tang, Prog. Theor. Phys. **93**, 711 (1995).
[22] G. R. Satchler, *Direct Nuclear Reactions* (Oxford University Press, New York, 1983).
[23] J. Raynal and R. Schaeffer, DWBA70 (unpublished).